

Phenology Dynamics of Dryland Ecosystems Along the North Australian Tropical Transect Revealed by Satellite Solar-Induced Chlorophyll Fluorescence

Wang, Cong; Beringer, Jason; Hutley, Lindsay B.; Cleverly, James; Li, Jing; Liu, Qinhua; Sun, Ying

Published in:
Geophysical Research Letters

DOI:
[10.1029/2019GL082716](https://doi.org/10.1029/2019GL082716)

Published: 28/05/2019

Document Version
Publisher's PDF, also known as Version of record

[Link to publication](#)

Citation for published version (APA):

Wang, C., Beringer, J., Hutley, L. B., Cleverly, J., Li, J., Liu, Q., & Sun, Y. (2019). Phenology Dynamics of Dryland Ecosystems Along the North Australian Tropical Transect Revealed by Satellite Solar-Induced Chlorophyll Fluorescence. *Geophysical Research Letters*, 46(10), 5294-5302.
<https://doi.org/10.1029/2019GL082716>

General rights

Copyright and moral rights for the publications made accessible in the public portal are retained by the authors and/or other copyright owners and it is a condition of accessing publications that users recognise and abide by the legal requirements associated with these rights.

- Users may download and print one copy of any publication from the public portal for the purpose of private study or research.
- You may not further distribute the material or use it for any profit-making activity or commercial gain
- You may freely distribute the URL identifying the publication in the public portal

Take down policy

If you believe that this document breaches copyright please contact us providing details, and we will remove access to the work immediately and investigate your claim.

Geophysical Research Letters

RESEARCH LETTER

10.1029/2019GL082716

Key Points:

- Satellite SIF matches seasonal phenology of eddy covariance GPP better than EVI and NIRv along a rainfall gradient in northern Australia
- Increasing soil exposure in inland xeric shrublands deteriorates the capability of satellite EVI and NIRv for phenology characterization
- High-resolution satellite SIF is needed to accurately depict phenology in heterogeneous landscapes with complex vegetation-soil mosaic

Supporting Information:

- Supporting Information S1

Correspondence to:

Y. Sun,
ys776@cornell.edu

Citation:

Wang, C., Beringer, J., Hutley, L. B., Cleverly, J., Li, J., Liu, Q., & Sun, Y. (2019). Phenology dynamics of dryland ecosystems along the North Australian Tropical Transect revealed by satellite solar-induced chlorophyll fluorescence. *Geophysical Research Letters*, 46, 5294–5302. <https://doi.org/10.1029/2019GL082716>

Received 5 MAR 2019

Accepted 26 APR 2019

Accepted article online 2 MAY 2019

Published online 23 MAY 2019

Phenology Dynamics of Dryland Ecosystems Along the North Australian Tropical Transect Revealed by Satellite Solar-Induced Chlorophyll Fluorescence

Cong Wang^{1,2,3} , Jason Beringer⁴ , Lindsay B. Hutley⁵ , James Cleverly⁶ , Jing Li², Qinhua Liu^{2,3,7} , and Ying Sun¹ 

¹School of Integrative Plant Science, Soil and Crop Sciences Section, Cornell University, Ithaca, NY, USA, ²State Key Laboratory of Remote Sensing Science, Institute of Remote Sensing and Digital Earth, Chinese Academy of Sciences, Beijing, China, ³College of Resources and Environment, University of Chinese Academy of Sciences (UCAS), Beijing, China, ⁴School of Agriculture and Environment, University of Western Australia, Crawley, Western Australia, Australia, ⁵School of Environment, Charles Darwin University, Darwin, Northern Territory, Australia, ⁶Terrestrial Ecosystem Research Network, School of Life Sciences, University of Technology Sydney, Sydney, New South Wales, Australia, ⁷Joint Center for Global Change Studies (JCGCS), Beijing, China

Abstract Accurate phenological characterization of dryland ecosystems has remained a challenge due to the complex composition of plant functional types, each having distinct phenological dynamics, sensitivity to climate, and disturbance. Solar-Induced chlorophyll Fluorescence (SIF), a proxy for photosynthesis, offers potential to alleviate such challenge. We here explore this potential using dryland systems along the North Australian Tropical Transect with SIF derived from Orbiting Carbon Observatory-2. SIF identified the seasonal onset and senescence of Gross Primary Production at eddy covariance sites with improved accuracy over Enhanced Vegetation Index and Near-Infrared Reflectance of terrestrial Vegetation from Moderate Resolution Imaging Spectroradiometer, especially at inland xeric shrublands. At regional scale, SIF depicted both earlier onset and senescence across North Australian Tropical Transect. We hypothesized that SIF outperformed Enhanced Vegetation Index and Near-Infrared Reflectance of terrestrial Vegetation mainly because, unlike reflectance, it is not contaminated by background soil, and its total signal is contributed by mixed plant species in additive way.

Plain Language Summary Australian dryland ecosystems are critical in regulating the global land carbon sink dynamics. However, it is challenging to accurately characterize their phenology from spaceborne measurements. On the one hand, tropical savannas and semiarid ecosystems (e.g., grasslands and shrublands) are typically composed of a complex mixture of species (woody trees and C₄ grasses) with each having distinct morphologies and physiological responses to climate condition; on the other hand, such ecosystems are highly sensitive to irregular rainfall events and are often subject to disturbances such as fires and storms. In this study, we utilized the North Australian Tropical Transect rainfall gradient as a “natural laboratory” to assess the ability of satellite solar-induced chlorophyll fluorescence to capture the phenological dynamics of dryland vegetation, in comparison with traditional reflectance-based vegetation indices, that is, Enhanced Vegetation Index and Near-Infrared Reflectance of terrestrial Vegetation. Results showed that satellite solar-induced chlorophyll fluorescence outperformed Enhanced Vegetation Index and Near-Infrared Reflectance of terrestrial Vegetation for characterizing seasonal onset and senescence along North Australian Tropical Transect and therefore had potential for improving large-scale mapping of phenology dynamics of dryland ecosystems over traditional remote sensing of reflectance-based vegetation indices.

1. Introduction

Australian dryland ecosystems play an important role in regulating the trend and interannual variability of the global land carbon sink (Ahlström et al., 2015; Poulter et al., 2014), mainly due to their strong sensitivity of ecosystem productivity (or Gross Primary Production [GPP]) to variation in climate and disturbance (Beringer et al., 2016; Chen et al., 2016; Ma et al., 2013). Accurate characterization of the phenology of dryland ecosystems, that is, the start and end dates of a growing season and the associated growing season

length, is critical for assessing the dynamics of carbon exchanges in these ecosystems. In Australia, environmental drivers, including both regular (e.g., rainfall and fire) and irregular (e.g., storms and cyclones) events, can alter ecosystem composition, structure, and functions (Moore et al., 2016). These features lead to high spatial heterogeneity of dryland vegetation productivity and a complex response to disturbance regimes and climate variability.

Satellite remote sensing of Solar-Induced chlorophyll Fluorescence (SIF) offers potential to unravel these complex ecosystem dynamics (Frankenberg et al., 2011). SIF is a signal emitted by green plants when solar photons are absorbed by chlorophylls within photosynthetic machinery, thus providing a mechanistic proxy for photosynthesis (Porcar-Castell et al., 2014). Satellite SIF retrievals have been demonstrated to be highly correlated with GPP at large scale and could be used to reveal GPP dynamics in response to environmental variations (e.g., Frankenberg et al., 2011; Guanter et al., 2012; Sun et al., 2017). Specific to dryland systems, studies have quantified the relationship between satellite SIF and GPP (e.g., Li, Xiao, & He, 2018; Li, Xiao, He, Altaf Arain, et al., 2018; Sanders et al., 2016; Smith et al., 2018; Verma et al., 2017). For example, Verma et al. (2017) found a robust linear correlation between NASA (National Aeronautics and Space Administration)'s Orbiting Carbon Observatory-2 (OCO-2) SIF and GPP derived from an eddy covariance (EC) flux tower at a semiarid grassland site in Australia over a season. Sanders et al. (2016) examined the SIF-GPP relationship of a number of EC towers in Australia using SIF records from the Global Ozone Monitoring Experiment-2 (GOME-2) onboard MetOp-A. They also found a linear SIF-GPP relationship but reported that managed biomes typically had higher correlations than natural vegetation. W. Smith et al. (2018) reported that for dryland systems in the southwest United States, GOME-2 SIF tended to better capture the seasonal and interannual variations in GPP than the traditional Enhanced Vegetation Index (EVI).

Although these studies demonstrated the correlation between SIF and GPP in space and time, the application of satellite SIF for elucidating the rapid phenological transitions of dryland vegetation has not yet been explored. The unique strength of SIF in depicting phenological transitions over conventional vegetation indices (VIs) has previously been reported for a diverse number of biomes (Joiner et al., 2014), primarily focusing on evergreen conifers, temperate forests, and crops (Jeong et al., 2017; Joiner et al., 2014; Lu et al., 2018; Urban et al., 2018; Walther et al., 2016). In contrast, phenology characterization for dryland ecosystems using SIF has not been conducted. The comparatively low productivity and thus lower SIF signal of dryland vegetation may suffer from relatively high noise level when using existing satellite SIF products (Sun et al., 2018). Moreover, the growth and phenology of dryland ecosystems are highly sensitive to irregular rainfall events (Brown et al., 2010; Eamus et al., 2013; Rogers & Beringer, 2017), in contrast to evergreen coniferous and temperate forests which are primarily driven by temperature variations. Consequently, an examination is needed to evaluate whether the weaker and noisier SIF signal in dryland ecosystems can still accurately detect phenology.

In this study, we defined dryland ecosystems in Australia as a structural continuum with varying mixtures of trees, grasses, and shrubs, including woodland savannas, shrublands, and grasslands, following Ma et al. (2013). We aim to (1) assess the ability of satellite SIF in capturing phenological dynamics of dryland systems and (2) determine the utility of SIF to advance phenological characterization in dryland ecosystems compared to the numerous current approaches that used reflectance-based VIs (e.g., Archibald & Scholes, 2007; Ferreira et al., 2013; Huete et al., 2002; Ma et al., 2013). To achieve this, we utilized the North Australian Tropical Transect (NATT) as a test bed, which provides a natural laboratory with wide range of vegetation structure, function, and phenological variability (Hutley et al., 2011; Mott et al., 1985; Williams et al., 1997). We compared SIF-based phenological metrics with those derived from EVI, which have previously been employed to characterize the phenology of Australian drylands (Broich et al., 2015; Ma et al., 2013). We also compared SIF with the recently developed Near-Infrared Reflectance of terrestrial Vegetation index (NIRv), that is, the product of total scene NIR reflectance and Normalized Difference Vegetation Index (NDVI), which was reported to be more closely coupled to GPP than NDVI alone, especially for sparsely vegetated areas (Badgley et al., 2017). This study did not include NDVI because it has already been demonstrated to be far more sensitive to soil background than EVI and NIRv (e.g., Badgley et al., 2017; Huete et al., 2002) and performed poorly in heterogeneous systems (Hmimina et al., 2013). We conducted our investigation first at EC towers along NATT and then scaled up the findings to the regional scale.

2. Data Sets and Methods

2.1. Site Characteristics and Measurements at Selected OzFlux EC Towers Along NATT

We selected six well-characterized EC tower sites from the OzFlux network (Gorsel et al., 2018) along NATT: Howard Springs (AU-How), Litchfield (AU-Lit), Daly River Uncleared (AU-Das), Dry River (AU-Dry), Stuart Plains (AU-Stp), and Alice Springs (AU-ASM; supporting information Figure S1 and Table S1; Beringer, Hacker, et al., 2011; Beringer, Hutley, et al., 2011; Cleverly et al., 2013; Hutley et al., 2011). These sites cover a transect from coastal humid savannas to inland arid/semiarid grasslands and shrublands (Figure S1a), with an increasing coverage of bare soil (Figure S1b).

At each site, we obtained half-hourly EC GPP between 2014 and 2018 from OzFlux. GPP fluxes were derived from the Dynamic Integrated Gap-filling and partitioning for OzFlux based on the level 3 data (Beringer et al., 2017). We aggregated half-hourly GPP to a 16-day composite to match the temporal resolution of the SIF products from OCO-2 (details in section 2.2.1). In addition, we used soil moisture (i.e., volumetric water content, m^3/m^3) measured at each EC site to examine the degree to which soil moisture impacted the temporal variation of vegetation activities. Here we used the top 10-cm soil moisture, because the depths of measurements vary from site to site and only the top layer (10 cm) is consistently available for all EC sites.

2.2. Description of Satellite Data Sets

2.2.1. OCO-2 SIF Products

We utilized both the native OCO-2 SIF (Sun et al., 2018) and spatially contiguous SIF products ($\overline{\text{SIF}}_{\text{OCO2}_005}$) at 0.05° and 16-day resolution gap-filled from OCO-2 by Yu et al. (2019), available since September 2014. OCO-2 SIF was retrieved at both 757 and 771 nm using solar Fraunhofer lines. This study used the average of the two wavelengths, with the 771 nm SIF scaled to 757 nm by a factor of 1.5 to reduce noise, following Sun et al. (2018). Here we extracted the native OCO-2 SIF pixels that (1) are within a 0.5° radius centered at each EC site, (2) are in nadir mode, and (3) have the same land cover type (details in section 2.2.2) as the EC tower. A relatively wide radius is required here to ensure sufficient number of retrievals for effectively reducing retrieval noise, although it will inevitably introduce scale mismatch between satellite and ground measurements. SIF values corresponding to each site were computed as the average of all extracted pixels. The instantaneous OCO-2 SIF was converted to daily averages using a daily correction factor (Sun et al., 2018).

This study primarily relied on $\overline{\text{SIF}}_{\text{OCO2}_005}$, a global spatially contiguous daily-average SIF product, for phenological characterization, because the existing native SIF retrievals have either spatial gaps (thus leading to lack of overlap with EC towers, e.g., OCO-2) or low spatial resolution (thus challenging to be applied to examine the highly dynamic dryland systems that are commonly spatially heterogeneous, e.g., GOME-2). $\overline{\text{SIF}}_{\text{OCO2}_005}$ is generated by a machine learning method constrained by physiological understandings and could accurately preserve the spatiotemporal variability of the original OCO-2 SIF across the globe (Yu et al., 2019). $\overline{\text{SIF}}_{\text{OCO2}_005}$ has been validated with independent airborne measurements from Chlorophyll Fluorescence Imaging Spectrometer. The spatial contiguity of $\overline{\text{SIF}}_{\text{OCO2}_005}$ makes it possible to examine the phenological synchrony of satellite SIF with in situ GPP, in contrast to the native OCO-2 SIF that are only available along orbits, which precludes the use of EC towers that are not directly underpassing OCO-2. Indeed, only AU-Stp (Verma et al., 2017), among the six selected sites along NATT, was in direct underpass of OCO-2 orbits. Also, lower data availability of the native OCO-2 SIF product prevented time series fitting for deriving phenological metrics (details in section 2.3). For each EC site, we averaged all $\overline{\text{SIF}}_{\text{OCO2}_005}$ pixels if (1) they have the same land cover type as the EC tower and (2) they are within a 3×3 window centered at the EC tower. In addition, $\overline{\text{SIF}}_{\text{OCO2}_005}$ was also used for spatial mapping of phenological metrics at the regional scale, which is not possible with the native OCO-2 SIF retrievals due to substantial orbital gaps.

2.2.2. MODIS EVI, NIRv, and Land Cover Type

Both EVI and NIRv in this study were computed from the Moderate Resolution Imaging Spectroradiometer (MODIS) Terra Vegetation Indices (MOD13C1, V006) at 0.05° and 16-day resolution. We used the ninth day of each 16-day composite period for each time stamp for subsequent phenology calculations. For each EC site, we averaged all pixels if (1) they have the same land cover type as the EC tower, (2) they are within a 3×3 window centered at the EC tower, and (3) they are in high quality according to the Quality Assurance flag. The land cover type was determined from the MCD12C1 V005 product at 0.05° resolution.

2.2.3. Soil fractional coverage

In order to assess the impact of background bare soil on phenological characterization, we used soil fractional coverage product developed by the Commonwealth Scientific and Industrial Research Organization. This data set is derived from the MODIS Nadir BRDF (Bidirectional Reflectance Distribution Function)-Adjusted Reflectance with a linear unmixing methodology (Guerschman et al., 2015). This product is provided monthly at 0.25°. Here we calculated the annual mean fraction of bare soil from monthly data sets in 2015.

2.3. Phenological Metrics

We employed the Singular Spectrum Analysis (SSA; Elsner & Tsonis, 1996) to smooth the time series and to derive the phenological metrics. SSA essentially uses the Singular Value Decomposition approach to reconstruct the time series from an originally noisy data set. This approach selects the leading Singular Value Decomposition components that contain most of the information of the trend and periodicity of the time series. The SSA approach is particularly suitable here for Australian dryland systems where satellite measurements are usually noisy (especially SIF) or interspersed with missing values due to cloud or aerosol contamination (such as EVI and NIRv). Ma et al. (2013) have successfully employed SSA to derive phenological metrics using EVI in northern Australia. This study adopted this approach and applied it to EC GPP, $\overline{\text{SIF}}_{\text{OCO2}_005}$, and MODIS NIRv and EVI. Here we set the window length as 24 consistently for all variables to capture the periodicity of phenology and reduce most of the random noise. We selected the first three leading components to reconstruct the time series. Three key phenological metrics were extracted for each variable: the start of growing season (SOS), defined as the date halfway between the minimum value and the fastest greening rate; the end of growing season (EOS), the date halfway between the fastest brown-down rate and minimum value; and the length of growing season, the difference between EOS and SOS.

3. Results and Discussions

3.1. Seasonal Variation and Phenological Metrics Extracted from SIF, EVI, NIRv, and GPP at EC Sites

The six EC sites showed distinct seasonality of GPP along NATT (Figure 1), with declining seasonal amplitude of GPP from the northern mesic savanna to the xeric shrublands, consistent with previous studies (Beringer et al., 2016; Ma et al., 2013). $\overline{\text{SIF}}_{\text{OCO2}_005}$ exhibited a stronger temporal consistency with EC GPP than EVI or NIRv did at most EC sites, evidenced by a greater R^2 of GPP with SIF than with EVI or NIRv from 2014 to 2018 (Figure 1). In particular, $\overline{\text{SIF}}_{\text{OCO2}_005}$ substantially outperformed EVI and NIRv at the xeric shrubland site AU-ASM, where the former captured more than 50% of the variability in GPP fluxes while the latter could only explain less than 20% (Figure 1f). However, the correlation between SIF and GPP appeared to degrade for AU-Dry (Figure 1d). This site is located near the center of orbital gaps where very few native OCO-2 measurements were acquired. Therefore, $\overline{\text{SIF}}_{\text{OCO2}_005}$ at this site might be more susceptible to uncertainties associated with gap-filling because of the long distance of the EC tower from orbits. Interestingly, both MODIS EVI and NIRv were very similar both intra-annually and interannually and exhibited similar R^2 with EC GPP although NIRv was designed to better characterize GPP dynamics for sparse vegetation (Badgley et al., 2017) such as dryland systems. We further found that $\overline{\text{SIF}}_{\text{OCO2}_005}$ tended to exhibit stronger consistency (i.e., greater R^2) with soil moisture than EC GPP, EVI, or NIRv did at most EC sites from 2014 to 2018 (Table S2).

We further evaluated the phenological metrics derived from $\overline{\text{SIF}}_{\text{OCO2}_005}$, EVI, and NIRv by comparing their deviation from GPP-derived phenology for each EC site (Table 1). Such deviation was evaluated using the mean absolute error across years. In general, there was considerable year-to-year and site-to-site variability of phenology depicted by satellite measurements, agreeing with Ma et al. (2013). At the northernmost mesic sites (i.e., AU-How and AU-Lit), SOS was similar among SIF, EVI, and NIRv, indicating their similar capability for monitoring the timing of seasonal green-up. Similar patterns were found for EOS at AU-How and AU-Das. The largest discrepancies of both SOS and EOS were observed at AU-Stp and AU-ASM (Table 1), where EVI and NIRv exhibited a substantial delay relative to GPP. In particular, at AU-ASM, EVI-based metrics were delayed by up to 84 days delay at SOS (40 days delay at EOS) relative to EC GPP, a magnitude comparable to Ma et al. (2013). In contrast, SIF appeared to have a closer correspondence with GPP at this site, with mean absolute error less than 20 days for SOS and EOS compared to GPP.

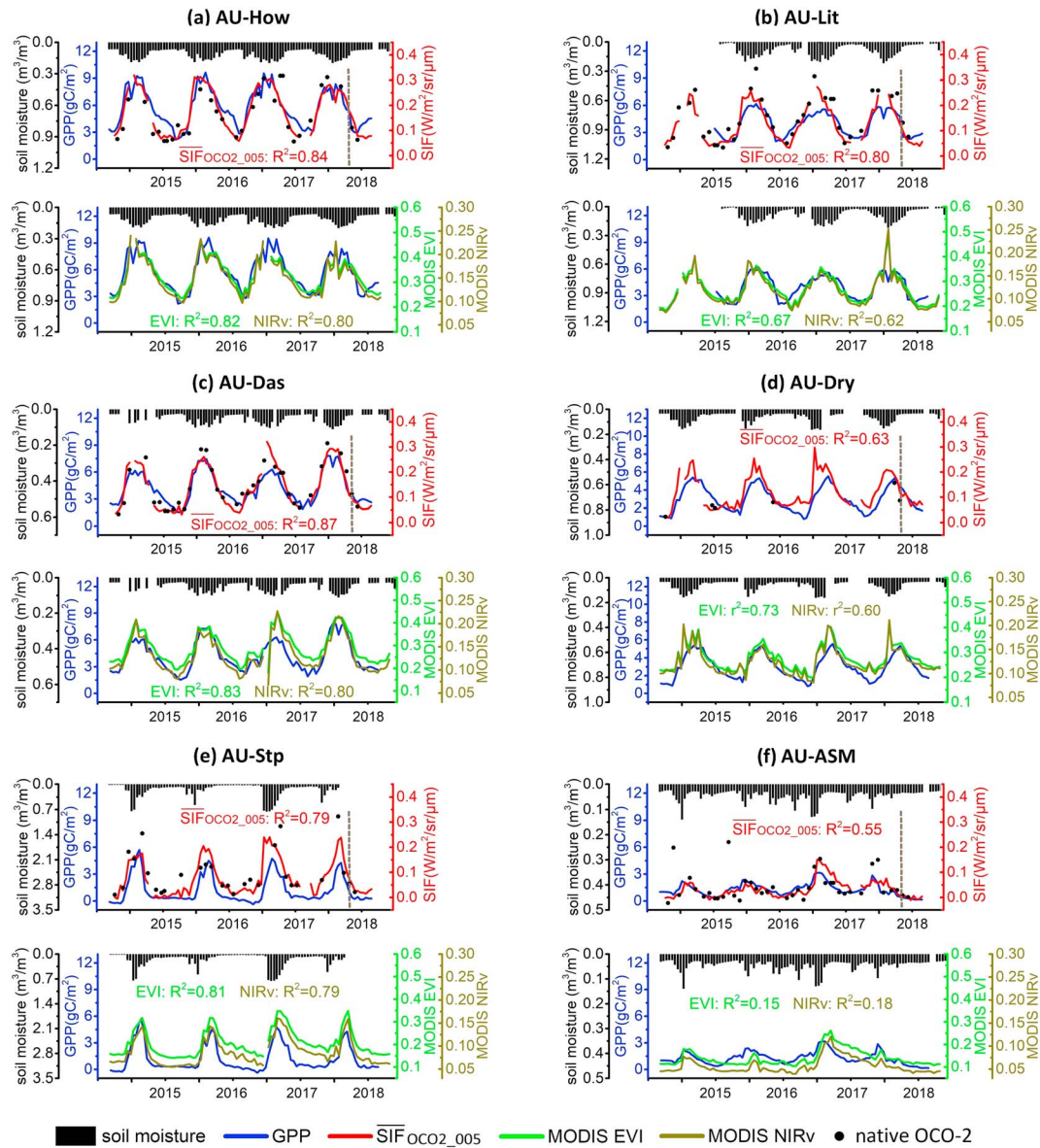


Figure 1. Time series of 16-day aggregated values at selected Ozflux eddy covariance towers along North Australian Tropical Transect: (a) AU-How (Howard Springs); (b) AU-Lit (Litchfield); (c) AU-Das (Daly River Uncleared); (d) AU-Dry (Dry River); (e) AU-Stp (Stuart Plains); (f) AU-ASM (Alice Springs). R^2 refers to the coefficients of determination from linear regressions between eddy covariance GPP and remote sensing variables. The dotted line highlights the month when TROPospheric Monitoring Instrument SIF retrievals became available. Note there are very few native OCO-2 SIF retrievals covering AU-Dry. GPP = Gross Primary Production; SIF = Solar-Induced chlorophyll Fluorescence; MODIS = Moderate Resolution Imaging Spectroradiometer; EVI = Enhanced Vegetation Index; NIRv = Near-Infrared Reflectance of terrestrial Vegetation; OCO-2 = Orbiting Carbon Observatory-2.

One possible reason is that the large soil coverage would have contaminated the reflectance-based VIs such as EVI and NIRv at this site. Indeed, AU-Asm, among all sites, has the largest soil fraction (Figure S1b). However, SIF contains zero contribution from nonfluorescing targets, as discussed in detail in section 3.2. These findings are consistent with the higher R^2 between SIF and GPP in Figure 1. An exception occurred at AU-Dry where EVI and NIRv outperformed SIF in identifying the SOS and EOS of GPP, again probably because of potential uncertainties present in $\overline{\text{SIF}}_{\text{OCO2_005}}$ originated from gap-filling, as explained above.

3.2. Spatial Patterns of Vegetation Phenology Across the NATT at the Regional Scale

To scale up our findings from individual EC sites, we utilized $\overline{\text{SIF}}_{\text{OCO2_005}}$, EVI, and NIRv to derive regional maps of SOS and EOS across the NATT (Figure 2). We observed a delaying pattern in both SOS and EOS

Table 1Summary of Differences (in Days) of SOS and EOS Derived From $\overline{\text{SIF}}_{\text{OCO2}_{005}}$, NIRv, and EVI, Relative to That Derived From GPP

| Site | Data | SOS | | | | EOS | | | | |
|--------|----------|-----------|-----------|-----------|--------------|-----------|-----------|-----------|-----------|--------------|
| | | 2015–2016 | 2016–2017 | 2017–2018 | MAE | 2014–2015 | 2015–2016 | 2016–2017 | 2017–2018 | MAE |
| AU-How | SIF-GPP | −8 | 2 | −6 | 5.33 | −36 | −20 | −8 | 9 | 18.25 |
| | NIRv-GPP | 7 | −10 | −6 | 7.67 | −20 | −10 | 1 | 25 | 14.00 |
| | EVI-GPP | 12 | −9 | −6 | 9.00 | −12 | −2 | 1 | 31 | 11.50 |
| AU-Lit | SIF-GPP | −16 | −1 | −9 | 8.67 | | −17 | −23 | −7 | 15.67 |
| | NIRv-GPP | −9 | −2 | −5 | 5.33 | | 0 | −7 | −5 | 4.00 |
| | EVI-GPP | −9 | 6 | −11 | 8.67 | | 7 | −7 | 0 | 4.67 |
| AU-Das | SIF-GPP | −7 | 0 | −3 | 3.33 | −39 | 0 | −6 | 8 | 13.25 |
| | NIRv-GPP | −2 | 31 | 4 | 12.33 | −22 | 17 | 12 | 9 | 15.00 |
| | EVI-GPP | −1 | 33 | 6 | 13.33 | −14 | 17 | 16 | 9 | 14.00 |
| AU-Dry | SIF-GPP | −37 | −37 | −38 | 37.33 | −53 | −16 | −15 | | 28.00 |
| | NIRv-GPP | 0 | 5 | −5 | 3.33 | −22 | 5 | −10 | | 12.33 |
| | EVI-GPP | 1 | 2 | 2 | 1.67 | −20 | 4 | −5 | | 9.67 |
| AU-Stp | SIF-GPP | −5 | −24 | −10 | 13.00 | −9 | −7 | −8 | | 8.00 |
| | NIRv-GPP | 22 | 15 | 29 | 22.00 | 8 | 10 | 10 | | 9.33 |
| | EVI-GPP | 30 | 15 | 28 | 24.33 | 26 | 11 | 10 | | 15.67 |
| AU-ASM | SIF-GPP | 11 | 26 | | 18.50 | −1 | 30 | | | 15.50 |
| | NIRv-GPP | 56 | 33 | | 44.50 | 38 | 34 | | | 36.00 |
| | EVI-GPP | 84 | 40 | | 62.00 | 39 | 40 | | | 39.50 |

Note. Negative values indicate that the variable of interest has an earlier onset (for SOS) or offset (for EOS) than that of GPP and vice versa. Values in bold highlight the smallest deviation from GPP-based phenological metrics among $\overline{\text{SIF}}_{\text{OCO2}_{005}}$, EVI, and NIRv. The MAE across years summarizes the overall discrepancy of SOS and EOS between each variable and GPP. Note that the missing SOS and EOS values for AU-Dry, AU-Stp, and AU-ASM in later years were primarily caused by incomplete time series that prevented successful Singular Spectrum Analysis fitting. AU-How = Howard Springs; AU-Lit = Litchfield; AU-Das = Daly River Uncleared; AU-Dry = Dry River; AU-Stp = Stuart Plains; AU-ASM = Alice Springs; SOS = start of growing season; EOS = end of growing season; SIF = Solar-Induced chlorophyll Fluorescence; EVI = Enhanced Vegetation Index; NIRv = Near-Infrared Reflectance of terrestrial Vegetation; GPP = Gross Primary Production; MAE = mean absolute error.

from the mesic north to the xeric south for all variables (Figure S2), consistent with the latitudinal shift reported by Ma et al. (2013). As expected, there was a striking consistency between EVI and NIRv in SOS, EOS, and length of growing season (Figure S2).

Interestingly, we found substantial differences between SIF and EVI (similarly NIRv) in the derived phenological metrics (Figure 2), which might be a consequence of the susceptibility of EVI and NIRv to high

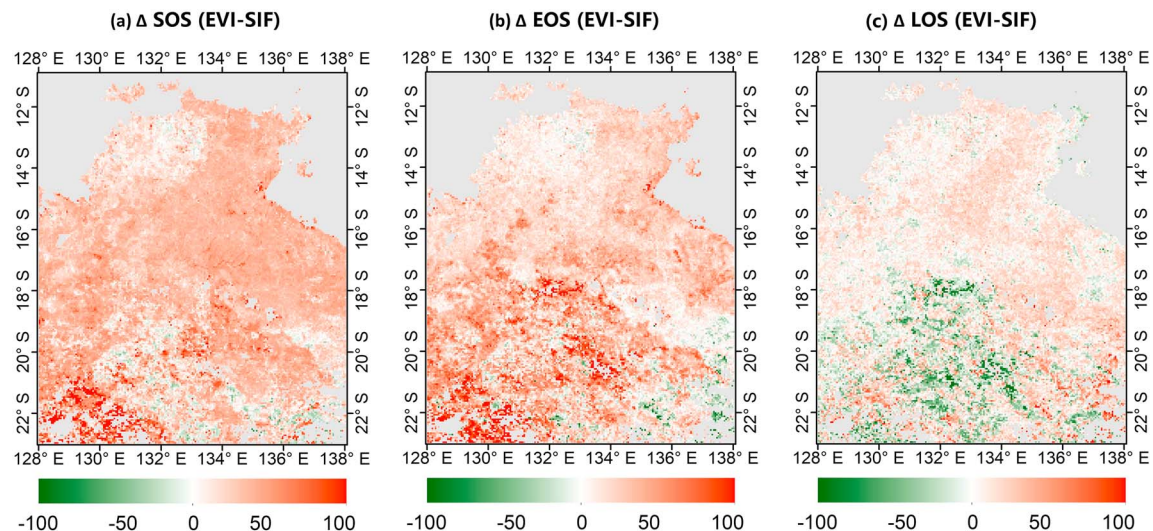


Figure 2. Spatial patterns of the differences of mean phenological metrics between EVI and $\overline{\text{SIF}}_{\text{OCO2}_{005}}$ (days) from 2015 to 2017, denoted as (a) ΔSOS , (b) ΔEOS , and (c) ΔLOS . SIF = Solar-Induced chlorophyll Fluorescence; EVI = Enhanced Vegetation Index; SOS = start of growing season; EOS = end of growing season; LOS = length of growing season.

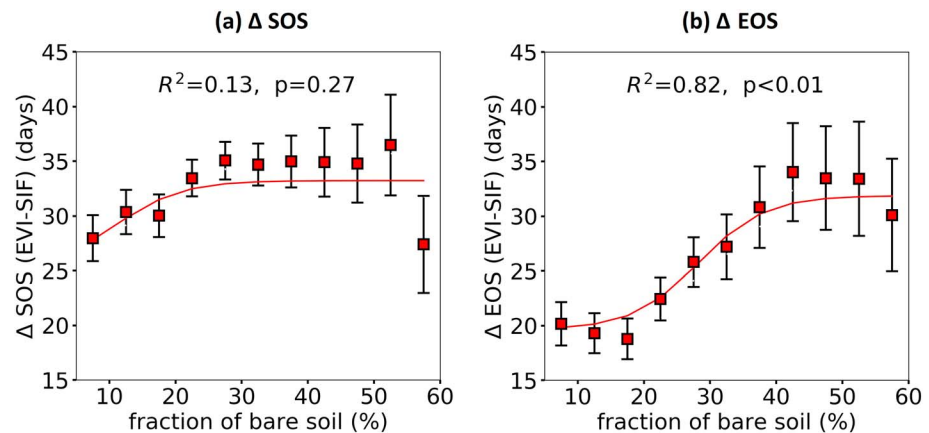


Figure 3. The relationship of (a) Δ SOS and (b) Δ EOS between EVI and $\overline{\text{SIF}}_{\text{OCO2}_{005}}$ with bare soil fraction. Data sets in Figure 2 were binned into bare soil fraction categories. The red squares and error bars represent the mean and standard error of each bin. The red line shows the nonlinear fit for the mean of each bin using logistic functions. SIF = Solar-Induced chlorophyll Fluorescence; EVI = Enhanced Vegetation Index; SOS = start of growing season; EOS = end of growing season.

heterogeneity in the mixture of soil type/texture and vegetation species (among other factors such as fires) that may confound the spectral signature of optical reflectance. To test this possibility, we computed the differences of SOS (and EOS) between EVI and $\overline{\text{SIF}}_{\text{OCO2}_{005}}$, denoted as Δ SOS (Δ EOS), and found that increasing soil exposure could result in larger Δ SOS and Δ EOS. Such dependence was statistically significant for Δ EOS ($R^2 = 0.82$, $p < 0.01$, Figure 3b), which could explain the increasing delay of EVI EOS relative to SIF toward the inland xeric shrublands in Figure 2b. This examination is useful to interpret the advantage of SIF for characterizing phenology of dryland systems. For reflectance, there is differential contribution of mixed plant species as well as soil to the total observed signal (Smith et al., 1990). However, SIF does not suffer from these issues, since (a) nonfluorescing targets (such as soil) do not contribute to the observed SIF signal and (b) different plant species contribute to the total SIF in additive way, which is not the case for optical reflectance (Frankenberg et al., 2014). The aggregated reflectance-based VIs from mixed species and soil do not necessarily linearly translate to aggregated GPP in the same footprint. Another plausible reason is that the reflectance-based VIs may only capture morphological development but not physiological responses of plant canopies. Therefore, any time lag between morphological and physiological changes could lead to a bias in phenological estimation (Joiner et al., 2014), which is particularly crucial for dryland systems that typically comprise a complex mixture of species which have distinct morphological traits and physiological responses to climate conditions. This may contribute to the insignificant relationship between Δ SOS and soil fraction in Figure 3a.

3.3. Outlook for Future Work

Future work is needed to further improve the accuracy of tracking phenological transitions with SIF. Achieving this will require higher spatial and temporal resolution SIF with less noise. Yu et al. (2019) reported that $\overline{\text{SIF}}_{\text{OCO2}_{005}}$ tended to underpredict high values and overpredict low values of SIF although the mean value was well predicted for shrubland. This may have resulted from the lower magnitude of SIF and thus higher impact of SIF retrieval noise in shrublands. In addition, the relatively coarse temporal resolution (16 days) could mask rapid changes in both SIF and VIs driven by high rainfall variability and may also influence SSA fitting, whose robustness will benefit from higher frequency data sets. SIF retrievals from Tropospheric Monitoring Instrument (TROPOMI; Köhler et al., 2018), which has a daily revisit cycle, may significantly improve the phenological characterization, although this study did not directly employ TROPOMI SIF as its mission period is too short (data available since March 2018) to conduct similar phenology analysis. This study did not attempt to separate trees and grasses to obtain their individual phenology dynamics because SIF itself as well as GPP is an integrated measure contributed by all vegetation components, with distinct morphology and function mixed within a pixel. Furthermore, the kilometer-scale resolution of SIF is not sufficient to accurately decouple the highly heterogeneous composition of woody and

herbaceous species, a challenge similarly faced by MODIS VIs (Ma et al., 2013). On the other hand, the unique features of SIF as an integrated proxy for GPP greatly simplify the needs to explicitly separate trees and grasses.

4. Conclusions

This study demonstrated that satellite SIF is capable of improving large-scale mapping and characterization of phenology dynamics of dryland ecosystems over traditional remote sensing of VIs, including EVI and NIRv. The main advantage of SIF lies in that, in contrast to reflectance-based VIs, it does not suffer from contamination of background soil, and its total signal is contributed by different plant species in additive way. This greatly alleviates the challenges for depicting phenology dynamics of dryland vegetation which is highly heterogeneous with complex vegetation-soil mosaic. While this study used the NATT as a test bed, it should have global implications and could be extended to other dryland ecosystems. Future applications of satellite SIF in phenological studies will further benefit from the next generation of sensor deployment from missions with higher spatial and/or temporal resolutions such as TROPOMI or the upcoming FLuorescence EXplorer.

Acknowledgments

C. Wang is supported by UCAS Joint PhD Training Program, National Key Research and Development Program (2018YFA0605503), and GF6 Project under grant 30-Y20A03-9003-17/18; Y. Sun is supported by the NASA MEaSURE program. The OzFlux network is supported by the Australian Government through the Terrestrial Ecosystem Research Network (TERN) and the National Collaborative Research Infrastructure Strategy (NCRIS). Ozflux GPP comes from an online website (<http://data.ozflux.org.au/portal/home.jsp>), SIF_{OCO2_005} is available online (<https://cornell.app.box.com/s/cavt50y80udbdirg022gm5whugmth02>), the native OCO-2 SIF is available online (<https://co2.jpl.nasa.gov>), all MODIS products come from an online website (<https://e4ftl01.cr.usgs.gov/MOTA/>), and the Fractional Cover data set is from an online website (http://qld.auscover.org.au/public/data/modis/fractional_cover/global/).

References

- Ahlström, A., Raupach, M. R., Schurgers, G., Smith, B., Arneth, A., Jung, M., et al. (2015). The dominant role of semi-arid ecosystems in the trend and variability of the land CO₂ sink. *Science*, 348(6237), 895–899. <https://doi.org/10.1126/science.aaa1668>
- Archibald, S., & Scholes, R. (2007). Leaf green-up in a semi-arid African savanna-separating tree and grass responses to environmental cues. *Journal of Vegetation Science*, 18(4), 583–594.
- Badgley, G., Field, C. B., & Berry, J. A. (2017). Canopy near-infrared reflectance and terrestrial photosynthesis. *Science Advances*, 3(3), e1602244. <https://doi.org/10.1126/sciadv.1602244>
- Beringer, J., Hacker, J., Hutley, L. B., Leuning, R., Arndt, S. K., Amiri, R., et al. (2011). SPECIAL—Savanna patterns of energy and carbon integrated across the landscape. *Bulletin of the American Meteorological Society*, 92(11), 1467–1485. <https://doi.org/10.1175/2011BAMS2948.1>
- Beringer, J., Hutley, L. B., Hacker, J. M., & Neininger, B. (2011). Patterns and processes of carbon, water and energy cycles across northern Australian landscapes: From point to region. *Agricultural and Forest Meteorology*, 151(11), 1409–1416. <https://doi.org/10.1016/j.agrformet.2011.05.003>
- Beringer, J., Hutley, L. B., McHugh, I., Arndt, S. K., Campbell, D., Cleugh, H. A., et al. (2016). An introduction to the Australian and New Zealand flux tower network—OzFlux. *Biogeosciences*, 13(21), 5895–5916. <https://doi.org/10.5194/bg-13-5895-2016>
- Beringer, J., McHugh, I., Hutley, L. B., Isaac, P., & Kljun, N. (2017). Dynamic INtegrated Gap-filling and partitioning for OzFlux (DINGO). *Biogeosciences*, 14(6), 1457–1460. <https://doi.org/10.5194/bg-14-1457-2017>
- Broich, M., Huete, A., Paget, M., Ma, X., Tulbure, M., Coupe, N. R., et al. (2015). A spatially explicit land surface phenology data product for science, monitoring and natural resources management applications. *Environmental Modelling & Software*, 64, 191–204. <https://doi.org/10.1016/j.envsoft.2014.11.017>
- Brown, M. E., de Beurs, K., & Vrieling, A. (2010). The response of African land surface phenology to large scale climate oscillations. *Remote Sensing of Environment*, 114(10), 2286–2296. <https://doi.org/10.1016/j.rse.2010.05.005>
- Chen, C., Cleverly, J., Zhang, L., Yu, Q., & Eamus, D. (2016). Modelling seasonal and inter-annual variations in carbon and water fluxes in an Arid-Zone Acacia Savanna Woodland, 1981–2012. *Ecosystems*, 19(4), 625–644. <https://doi.org/10.1007/s10021-015-9956-8>
- Cleverly, J., Boulain, N., Villalobos-Vega, R., Grant, N., Faux, R., Wood, C., et al. (2013). Dynamics of component carbon fluxes in a semi-arid Acacia woodland, central Australia. *Journal of Geophysical Research: Biogeosciences*, 118, 1168–1185. <https://doi.org/10.1002/jgrg.20101>
- Eamus, D., Cleverly, J., Boulain, N., Grant, N., Faux, R., & Villalobos-Vega, R. (2013). Carbon and water fluxes in an arid-zone Acacia savanna woodland: An analyses of seasonal patterns and responses to rainfall events. *Agricultural and Forest Meteorology*, 182–183, 225–238. <https://doi.org/10.1016/j.agrformet.2013.04.020>
- Elsner, J. B., & Tsonis, A. A. (1996). *Singular Spectrum Analysis: A New Tool in Time Series Analysis*. New York: Plenum.
- Ferreira, M. E., Ferreira, L. G. Jr., Miziara, F., & Soares-Filho, B. S. (2013). Modeling landscape dynamics in the central Brazilian savanna biome: Future scenarios and perspectives for conservation. *Journal of Land Use Science*, 8(4), 403–421. <https://doi.org/10.1080/1747423X.2012.675363>
- Frankenberg, C., Fisher, J. B., Worden, J., Badgley, G., Saatchi, S. S., Lee, J. E., et al. (2011). New global observations of the terrestrial carbon cycle from GOSAT: Patterns of plant fluorescence with gross primary productivity. *Geophysical Research Letters*, 38, L17706. <https://doi.org/10.1029/2011GL048738>
- Frankenberg, C., O'Dell, C., Berry, J., Guanter, L., Joiner, J., Köhler, P., et al. (2014). Prospects for chlorophyll fluorescence remote sensing from the Orbiting Carbon Observatory-2. *Remote Sensing of Environment*, 147, 1–12. <https://doi.org/10.1016/j.rse.2014.02.007>
- Gorsel, E. V., Cleverly, J., Beringer, J., Cleugh, H., Eamus, D., Hutley, L. B., et al. (2018). Preface: OzFlux: A network for the study of ecosystem carbon and water dynamics across Australia and New Zealand. *Biogeosciences*, 15(1), 349–352. <https://doi.org/10.5194/bg-15-349-2018>
- Guanter, L., Frankenberg, C., Dudhia, A., Lewis, P. E., Gómez-Dans, J., Kuze, A., et al. (2012). Retrieval and global assessment of terrestrial chlorophyll fluorescence from GOSAT space measurements. *Remote Sensing of Environment*, 121, 236–251. <https://doi.org/10.1016/j.rse.2012.02.006>
- Guerschman, J. P., Scarth, P. F., McVicar, T. R., Renzullo, L. J., Malthus, T. J., Stewart, J. B., et al. (2015). Assessing the effects of site heterogeneity and soil properties when unmixing photosynthetic vegetation, non-photosynthetic vegetation and bare soil fractions from Landsat and MODIS data. *Remote Sensing of Environment*, 161, 12–26. <https://doi.org/10.1016/j.rse.2015.01.021>

- Hmimina, G., Dufrêne, E., Pontailier, J.-Y., Delpierre, N., Aubinet, M., Caquet, B., et al. (2013). Evaluation of the potential of MODIS satellite data to predict vegetation phenology in different biomes: An investigation using ground-based NDVI measurements. *Remote Sensing of Environment*, 132, 145–158. <https://doi.org/10.1016/j.rse.2013.01.010>
- Huete, A., Didan, K., Miura, T., Rodriguez, E. P., Gao, X., & Ferreira, L. G. (2002). Overview of the radiometric and biophysical performance of the MODIS vegetation indices. *Remote Sensing of Environment*, 83(1–2), 195–213. [https://doi.org/10.1016/S0034-4257\(02\)00096-2](https://doi.org/10.1016/S0034-4257(02)00096-2)
- Hutley, L. B., Beringer, J., Isaac, P. R., Hacker, J. M., & Cernusak, L. A. (2011). A sub-continental scale living laboratory: Spatial patterns of savanna vegetation over a rainfall gradient in northern Australia. *Agricultural and Forest Meteorology*, 151(11), 1417–1428. <https://doi.org/10.1016/j.agrformet.2011.03.002>
- Jeong, S.-J., Schimel, D., Frankenberg, C., Drewry, D. T., Fisher, J. B., Verma, M., et al. (2017). Application of satellite solar-induced chlorophyll fluorescence to understanding large-scale variations in vegetation phenology and function over northern high latitude forests. *Remote Sensing of Environment*, 190, 178–187. <https://doi.org/10.1016/j.rse.2016.11.021>
- Joiner, J., Yoshida, Y., Vasilkov, A., Schaefer, K., Jung, M., Guanter, L., et al. (2014). The seasonal cycle of satellite chlorophyll fluorescence observations and its relationship to vegetation phenology and ecosystem atmosphere carbon exchange. *Remote Sensing of Environment*, 152, 375–391. <https://doi.org/10.1016/j.rse.2014.06.022>
- Köhler, P., Frankenberg, C., Magney, T. S., Guanter, L., Joiner, J., & Landgraf, J. J. G. R. L. (2018). Global retrievals of solar-induced chlorophyll fluorescence with TROPOMI: First results and intersensor comparison to OCO-2. *Geophysical Research Letters*, 45(19), 10,456–10,463. <https://doi.org/10.1029/2018GL079031>
- Li, X., Xiao, J., & He, B. (2018). Chlorophyll fluorescence observed by OCO-2 is strongly related to gross primary productivity estimated from flux towers in temperate forests. *Remote Sensing of Environment*, 204, 659–671. <https://doi.org/10.1016/j.rse.2017.09.034>
- Li, X., Xiao, J., He, B., Altaf Arain, M., Beringer, J., Desai, A. R., et al. (2018). Solar-induced chlorophyll fluorescence is strongly correlated with terrestrial photosynthesis for a wide variety of biomes: First global analysis based on OCO-2 and flux tower observations. *Global Change Biology*, 24(9), 3990–4008. <https://doi.org/10.1111/gcb.14297>
- Lu, X., Liu, Z., Zhou, Y., Liu, Y., An, S., & Tang, J. (2018). Comparison of phenology estimated from reflectance-based indices and solar-induced chlorophyll fluorescence (SIF) observations in a temperate forest using GPP-based phenology as the standard. *Remote Sensing*, 10(6), 932. <https://doi.org/10.3390/rs10060932>
- Ma, X., Huete, A., Yu, Q., Coupe, N. R., Davies, K., Broich, M., et al. (2013). Spatial patterns and temporal dynamics in savanna vegetation phenology across the North Australian Tropical Transect. *Remote Sensing of Environment*, 139, 97–115. <https://doi.org/10.1016/j.rse.2013.07.030>
- Moore, C. E., Brown, T., Keenan, T. F., Duursma, R. A., Dijk, A. I. V., Beringer, J., et al. (2016). Reviews and syntheses: Australian vegetation phenology: New insights from satellite remote sensing and digital repeat photography. *Biogeosciences*, 13(17), 5085–5102. <https://doi.org/10.5194/bg-13-5085-2016>
- Mott, J., Williams, J., Andrew, M., & Gillison, A. (1985). Australian savanna ecosystems. In J. C. Tothill, & J. J. Mott (Eds.), *Ecology and management of the world's savannas* (pp. 56–82). Canberra, Australia: Australian Academy of Science.
- Porcar-Castell, A., Tyystjärvi, E., Atherton, J., Van der Tol, C., Flexas, J., Pfündel, E. E., et al. (2014). Linking chlorophyll a fluorescence to photosynthesis for remote sensing applications: Mechanisms and challenges. *Journal of Experimental Botany*, 65(15), 4065–4095. <https://doi.org/10.1093/jxb/eru191>
- Poulter, B., Frank, D., Ciais, P., Myneni, R. B., Andela, N., Bi, J., et al. (2014). Contribution of semi-arid ecosystems to interannual variability of the global carbon cycle. *Nature*, 509(7502), 600–603. <https://doi.org/10.1038/nature13376>
- Rogers, C. D. W., & Beringer, J. (2017). Describing rainfall in northern Australia using multiple climate indices. *Biogeosciences*, 14(3), 597–615. <https://doi.org/10.5194/bg-14-597-2017>
- Sanders, A. F., Verstraeten, W. W., Kooreman, M. L., Van Leth, T. C., Beringer, J., & Joiner, J. (2016). Spaceborne sun-induced vegetation fluorescence time series from 2007 to 2015 evaluated with Australian flux tower measurements. *Remote Sensing*, 8(11), 895. <https://doi.org/10.3390/rs8110895>
- Smith, M. O., Ustin, S. L., Adams, J. B., & Gillespie, A. R. (1990). Vegetation in deserts. I. A regional measure of abundance from multi-spectral images. *Remote Sensing of Environment*, 31(1), 1–26. [https://doi.org/10.1016/0034-4257\(90\)90074-V](https://doi.org/10.1016/0034-4257(90)90074-V)
- Smith, W., Biederman, J., Scott, R., Moore, D., He, M., Kimball, J., et al. (2018). Chlorophyll fluorescence better captures seasonal and interannual gross primary productivity dynamics across dryland ecosystems of southwestern North America. *Geophysical Research Letters*, 45(2), 748–757. <https://doi.org/10.1002/2017GL075922>
- Sun, Y., Frankenberg, C., Jung, M., Joiner, J., Guanter, L., Köhler, P., & Magney, T. (2018). Overview of solar-induced chlorophyll fluorescence (SIF) from the Orbiting Carbon Observatory-2: Retrieval, cross-mission comparison, and global monitoring for GPP. *Remote Sensing of Environment*, 209, 808–823. <https://doi.org/10.1016/j.rse.2018.02.016>
- Sun, Y., Frankenberg, C., Wood, J. D., Schimel, D. S., Jung, M., Guanter, L., et al. (2017). OCO-2 advances photosynthesis observation from space via solar-induced chlorophyll fluorescence. *Science*, 358(6360), eaam5747. <https://doi.org/10.1126/science.aam5747>
- Urban, D., Guan, K., & Jain, M. (2018). Estimating sowing dates from satellite data over the US Midwest: A comparison of multiple sensors and metrics. *Remote Sensing of Environment*, 211, 400–412. <https://doi.org/10.1016/j.rse.2018.03.039>
- Verma, M., Schimel, D., Evans, B., Frankenberg, C., Beringer, J., Drewry, D. T., et al. (2017). Effect of environmental conditions on the relationship between solar-induced fluorescence and gross primary productivity at an OzFlux grassland site. *Journal of Geophysical Research: Biogeosciences*, 122, 716–733. <https://doi.org/10.1002/2016JG003580>
- Walther, S., Voigt, M., Thum, T., Gonsamo, A., Zhang, Y., Köhler, P., et al. (2016). Satellite chlorophyll fluorescence measurements reveal large-scale decoupling of photosynthesis and greenness dynamics in boreal evergreen forests. *Global Change Biology*, 22(9), 2979–2996. <https://doi.org/10.1111/gcb.13200>
- Williams, R., Myers, B., Muller, W., Duff, G., & Eamus, D. (1997). Leaf phenology of woody species in a north Australian tropical savanna. *Ecology*, 78(8), 2542–2558. [https://doi.org/10.1890/0012-9658\(1997\)078\[2542:LPOWSI\]2.0.CO;2](https://doi.org/10.1890/0012-9658(1997)078[2542:LPOWSI]2.0.CO;2)
- Yu, L., Wen, J., Chang, C. Y., Frankenberg, C., & Sun, Y. (2019). High-resolution global contiguous SIF of OCO-2. *Geophysical Research Letters*, 46(3), 1449–1458.